

# The origin of hydrological responses following earthquakes in confined aquifer: Insight from water level, flow rate and temperature observations

5 Shouchuan Zhang<sup>1,2</sup>, Zheming Shi<sup>1\*</sup>, Guangcai Wang<sup>1</sup>, Zuochen Zhang<sup>3</sup>, Huaming Guo<sup>1</sup>  
<sup>1</sup>MOE Key Laboratory of Groundwater Circulation and Environmental Evolution, China University of Geosciences, Beijing, China  
<sup>2</sup>Chinese Academy of Geological Science, Beijing, China  
<sup>3</sup>Institute of Geomechanics, Chinese Academy of Geological Science, Beijing, China  
10 *Corresponding to: Zheming Shi (szm@cugb.edu.cn)*

## Contents of this file

1. Aquifer lithology and wellbore structure of Dazhai deep well aquifer system
2. The raw data of water level in Dazhai well
3. Spectral analysis of water level in Dazhai well
- 15 4. Fault-plane solutions for earthquakes
5. The accuracy and efficiency of model fitting results
6. The results of wavelet coherence analysis

## Text S1. Aquifer lithology and wellbore structure of Dazhai deep well aquifer system:

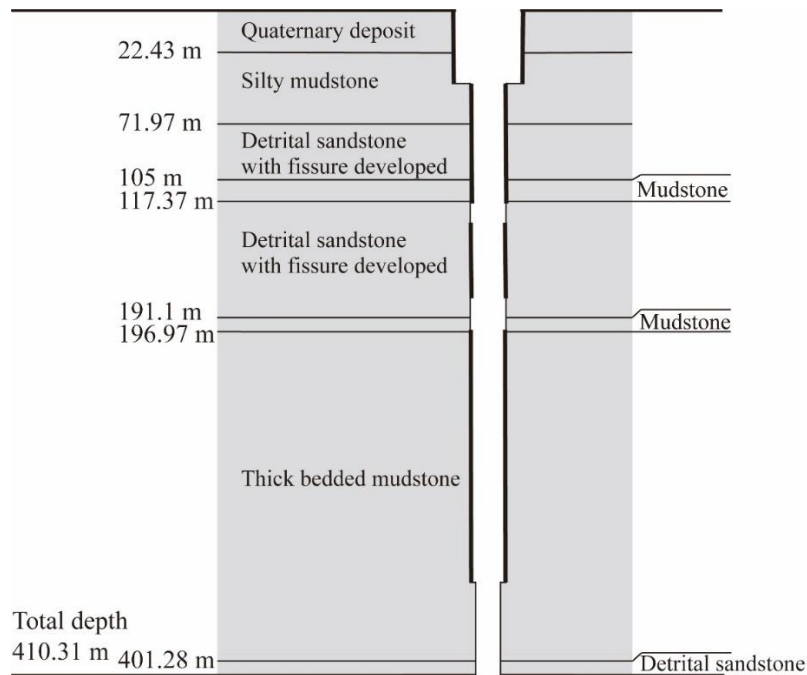


Figure S1. Aquifer lithology and wellbore structure of Dazhai deep well aquifer system.

25

The lithology of the wellbore in Dazhai deep well is as follow (Figure S1): 0m~22.43m is quaternary deposit, 22.43m~71.97m is silty mudstone, 71.97m~105m is detrital sandstone with fissure developed, 105m~117.37m is mudstone, 117.37m~191.10m is detrital sandstone with fissure developed, 191.10m~196.97m is mudstone, 196.97m~401.28m is thick bedded mudstone, and 401.28m~410.31m is detrital sandstone.

**Text S2. The raw data of water level in Dazhai well:**

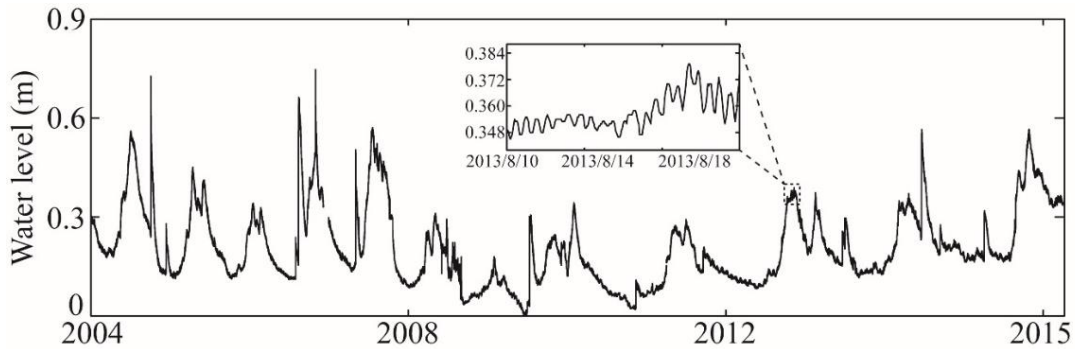


Figure S2. The raw data of water level in Dazhai well. The inset represents the zoom-in of the time series.

30

The raw data of water level is shown in Figure S2, and the inset is that the water level in Dazhai well shows responds to Earth tides.

**Text S3. Spectral analysis of water level in Dazhai well:**

35

The obvious amplitudes were observed in a frequency band of 0~3cpd (Figure S3), indicating that the water level in Dazhai well responds to Earth tides.

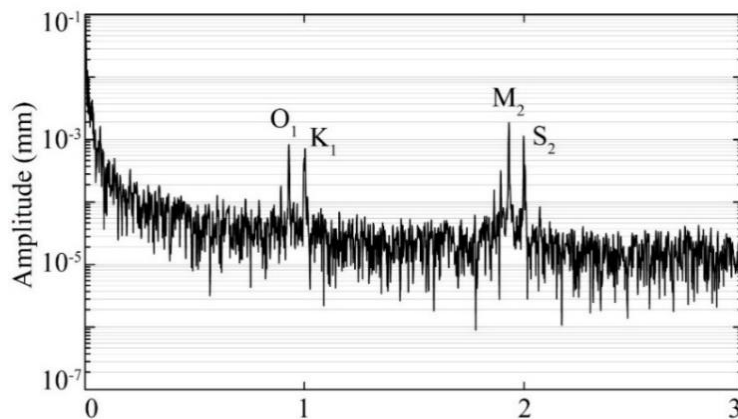
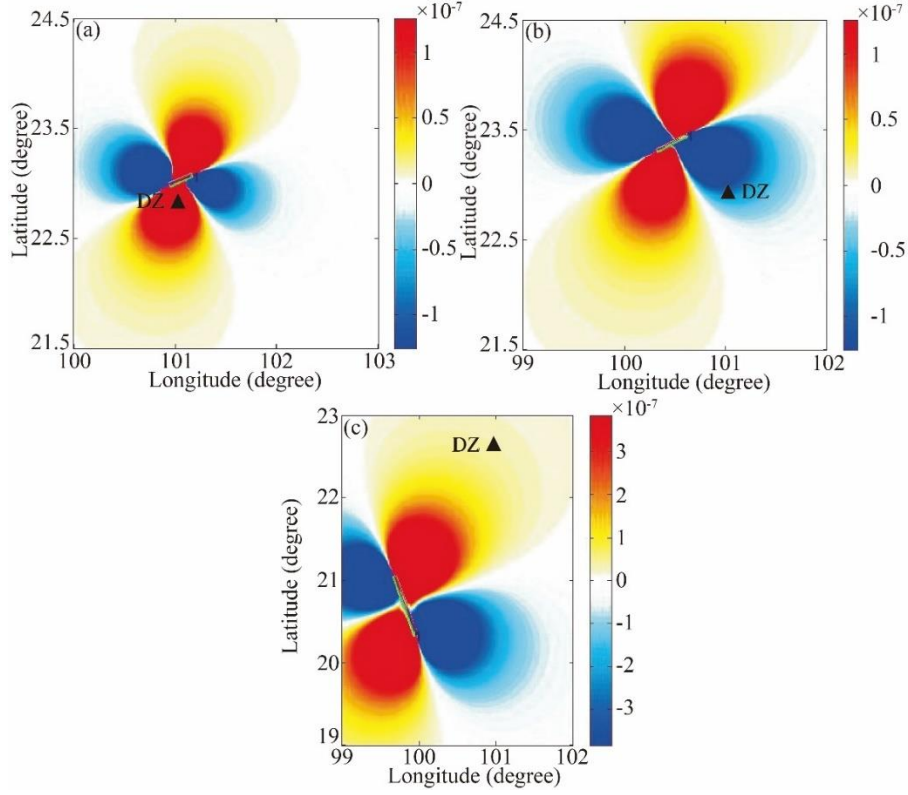


Figure S3. Amplitude spectrum for hourly water levels in Dazhai Well, western Yunnan Province, China.

**Text S4. Fault-plane solutions for earthquakes**



40 Figure S4. Coseismic static strain caused by (a) EQ4  $M_w$  6.4 2007/6/3, (b) EQ12  $M_w$  6.6 2014/10/7, and (c) EQ7  $M_w$  7.2 2011/3/24. Blue zones show contraction while the red zones indicate dilation. Location of Dazhai Well (DZ) indicated using black triangle.

Table S1. Fault-plane solutions for four earthquakes examined in this study.

Earthquake ID	Date	Hypocentral depth (km)	Strike ( $^{\circ}$ )	Dip ( $^{\circ}$ )	Rake ( $^{\circ}$ )
EQ4	Jun, 3 2007	5	247	69	30
EQ6	May, 12 2008	19	222	29	152
EQ7	Mar, 24 2011	8	340	77	176
EQ12	Oct, 7 2014	8.5	242	79	-7

#### 45 Text S5. The accuracy and efficiency of model fitting results

Three error metrics are conducted to evaluate the accuracy and efficiency of model fitting results, as follow:

Root mean square error (RMSE):

$$\text{RMSE} = \sqrt{\frac{\sum_{i=1}^N (y_i - y_i^*)^2}{N}} \quad (\text{S1})$$

50 The Nash-Sutcliffe efficiency (NSE):

$$\text{NSE} = 1 - \frac{\sum_{i=1}^N (y_i - y_i^*)^2}{\sum_{i=1}^N (y_i - \bar{y}_i)^2} \quad (\text{S2})$$

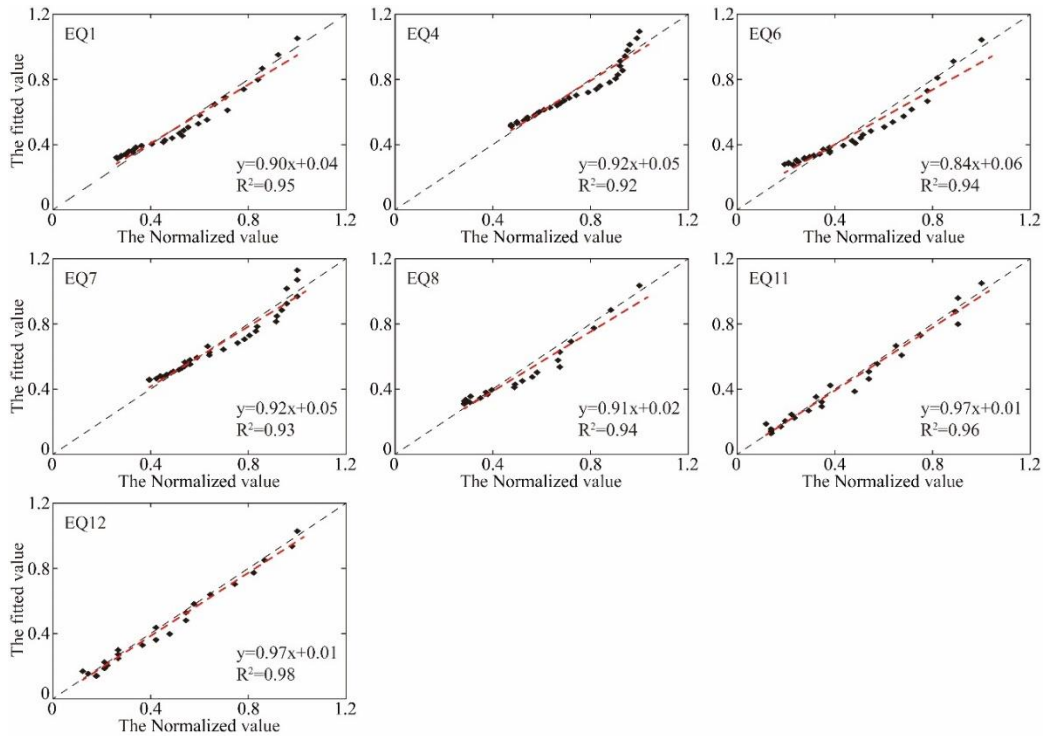
The coefficient of determination:

$$R^2 = 1 - \frac{\sum_{i=1}^N (y_i - y_i^*)^2}{\sum_{i=1}^N y_i^2 - \frac{\sum_{i=1}^N y_i^{*2}}{N}} \quad (S3)$$

55 where  $y_i$  is the observed value,  $y_i^*$  are the simulated value,  $\bar{y}_i$  is the mean of observed values and N the number of observations. The RMSE is the deviation between the observed and simulated values, and smaller values indicate a better model. NSE measures the model performance for training and testing, which is an efficiency indicator for hydrologic models. The value of NSE close to 1 represents the model predictability is satisfactory (Yoon et al., 2011).  $R^2$  is used to analyze the linear regression goodness of fit between observed and simulated value. When RMSE is close to 0, and NSE and  $R^2$  are close to 1, this model is regarded as a  
60 good fit between simulated and observed value.

Table S2. The models fitting errors following seven earthquakes.

Earthquake ID	Date	RMSE	NSE	$R^2$
EQ1	Dec, 26 2004	0.05	0.97	0.95
EQ4	Jun, 3 2007	0.05	0.98	0.92
EQ6	May, 12 2008	0.06	0.96	0.94
EQ7	Mar, 24 2011	0.05	0.98	0.93
EQ8	Apr, 11 2012	0.06	0.97	0.94
EQ11	Feb, 5 2014	0.05	0.95	0.96
EQ12	Oct, 7 2014	0.04	0.98	0.98



65

Figure S5. Scatter plot of the simulated and observed value. Gray dotted lines represent 1:1 line. The red solid lines dashed line represents the trend lines.

The scatter plot of the fitted and observed value is shown in Figure S5. The X-axis and Y-axis represent the observed value and simulated value respectively. Under the ideal condition, the prediction results should be distributed over  $X=Y$  or evenly distributed on both sides of the line. The closer the point to the  $X=Y$  line, the smaller the errors. The model fitted errors are summarized in Table S2. The RMSE of all models range from 0.04 to 0.06, the NSE value ranges from 0.83 to 0.98, and the  $R^2$  are greater than 0.84. Although the fitting results are not such perfect at the maximum value of discharge after earthquakes, the error analysis show that the errors evaluated by different methods are small and acceptable. Thus, we consider that our model is able to describe the co-seismic discharge processes following the different earthquakes.

**Text S5. The results of wavelet coherence analysis.**

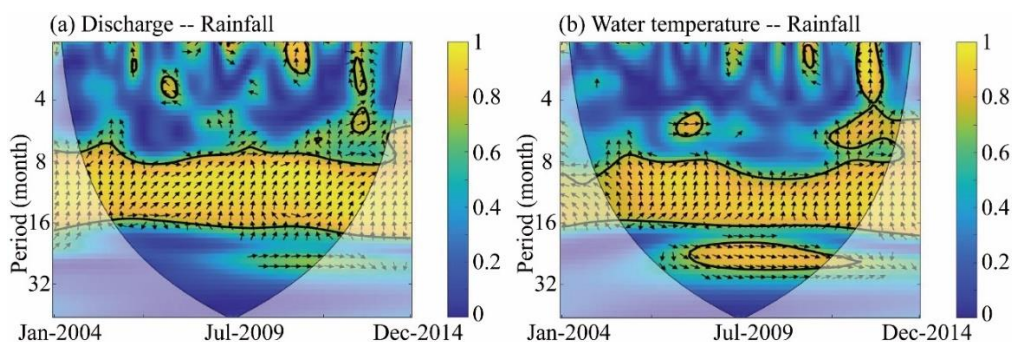


Figure S6. Wavelet coherence analysis between (a) discharge and rainfall (b) water temperature and rainfall. Thick black contour indicates the 95% confidence level and lighter shade indicates regions inside the cone of influence (COI). Arrows indicate the relative phase relationship (in-phase pointing right, anti-phase pointing left, and phase-leading by 90° pointing down).

**References:**

Yoon, H., Jun, S.-C., Hyun, Y., and Gwang-Ok: A comparative study of artificial neural networks and support vector machines for predicting groundwater levels in a coastal aquifer, *Journal of Hydrology*, 396, 128-138, <https://doi.org/10.1016/j.jhydrol.2010.11.002>, 2011.